Thermal Property Investigation of a Simplified, Dye-Sensitized Solar Cell: Analyzing the Heat Transfer in Solids and Fluids, with a Turbulent Flow, for Open-Circuit Voltage Calculations

Ervin Racz

Kando Kalman Faculty of Electrical Engineering, Obuda University, 1034 Budapest, Hungary, racz@uni-obuda.hu

Abstract: Utilizing renewable energy sources is a long-term mitigation solution. Electricity generation by photovoltaic (PV) is growing rapidly and PV is at the forefront of the renewable energy revolution. Dye-Sensitized Solar Cell (DSSC) is one of the more popular transparent solar cells used for architectures. Additionally, DSSC is a cost-effective solar cell and simple to manufacture because of the inexpensive materials, which are used in the fabrication processes. This article explores a method to optimize the thermal properties of the DSSC. For the simulation COMSOL Multiphysics software usage has been used and 3-dimensional scheme via numerically solved coupled models – such as heat transfer in solids and fluids, and turbulent flow – in stationary mode have been applied. Boundary conditions have been added and described in great details. For the optimization process, the glass substrate has been modified. The temperature distribution in the volume and in the surface; pressure distribution in the volume; and velocity distribution in the volume have been presented. On the other hand, the temperature distribution, along a line, is extracted from the 3-dimensional geometry, to analyze the thermal behavior and use for further investigation, the electrical behavior of the Dye-Sensitized Solar Cell. The results show that the higher temperature, which is located at the top part of the geometry, is 318 K. The calculated open-circuit voltage of the cell is between 448 mV and 452 mV and the gradient is $-2\ mV/°C$.

Keywords: Dye-Sensitized Solar Cell; Optimization; Thermal Analysis; Simulation; Open-Circuit Voltage

1 Introduction

The Global Energy Crisis is a high-level scientific challenge, which has not been solved. It is an intensely debated topic, concerning what kind of measurements have to be taken, in order to reduce carbon-dioxide emission into the atmosphere [1]. Devastating results are forecasted, if the current trends continue in electricity

production [2] [3]. Many researchers emphasized that the use of cost-effective, low-carbon energy technologies are very relevant and undisputedly important [4]. Furthermore, if this continues, carbon-dioxide emissions could be 60% higher within 25 years compared to the current emissions. The most significant greenhouse gas is carbon-dioxide. On the other hand, the energy demand is predicted to be 70% higher by 2050 [5]. Fossil fuel-based energy generation has been the dominant mode of energy production in previous decades, contributing a great deal of greenhouse gas emissions [6-8].

Utilizing renewable energy sources is a long-term mitigation solution. As a matter of fact, the electromagnetic radiation (waves) hit the earth's surface can significantly cover the needs of humans' activity [9]. This is why, solar energy is more urgent than ever before. On the other hand, billions of US dollars had been invested into clean energy development [10]. Moreover, electricity generation by photovoltaics (PV) is growing rapidly and PV is at the forefront of the renewable energy revolution [11]. The device harnesses the power of the electromagnetic wave and directly converts it into electrical energy. However, several solar cell types exist, the most commonly used photovoltaic device is the monocrystalline solar panel. The principle of the effect is that the striking photons excite the electrons in the semiconductor material, causing the generation and the flow of the electric current, known as direct current (DC) [12]. After that DC is converted into alternating current (AC) using inverters [13]. The current trends show that solar cell research also moved towards building integrated photovoltaic in which transparent solar cell is favorable [14].

Dye-sensitized solar cell (DSSC) is one of the most popular transparent solar cells used for architecture. Additionally, DSSC is a cost-effective solar cell and simple to manufacture solar cell because inexpensive materials are used for fabrication processes. DSSC is composed of five main components: glass substrate coated with transparent conductive oxide, titanium-dioxide semiconductor, dye sensitizer, electrolyte solution and platinum catalyst. The sensitizing dye molecules are excited by the incoming photons, then electrons injected from dye molecule into the conduction band of the titanium-dioxide semiconductor layer. The charge separation and charge generation are done separately. Moreover, after the injection, the dye is oxidized and it can receive electrons from the electrolyte solution. After, ions diffuse to the counter electrode in order to receive electrons [15]. The dye absorber has to meet with the following requirement: It has to be able to absorb a wide part of the solar spectrum. Interestingly, the number of publications has increased due to the intensive research interest towards this innovative cell [16].

Arifin et al. investigated the effect of heat sink properties on solar cell cooling system using numerical simulations and experimental investigation. In the study a passive cooling system, namely heat sink, has been added. The cooling system was modelled using Navier-Stokes equation. Applying 15 pins copper-based heat sink, the temperature of the solar cell decreased by 10.2 °C, and the efficiency of the PV increased by 2.74% [17]. Other researchers conducted analysis on dye-sensitized

solar cell and temperature improvement. Baiju et al. reported a temperature sintering process of titanium-dioxide on polymer substrates using heat sink [18]. Others proposed a dye-sensitized solar cell – thermoelectric hybrid system in order to improve the output efficiency and electric power of the system [19]. On the other hand, this innovative method also enhances the thermal effect of the solar cell by recycling the accumulated heat inside the DSSC. In the study of Chang. et al, a solar thermoelectric module investigation was doing by the integration of CuO thin films [20]. Chen et al. analyzed the thermal performance of a DSSC module using numerical model. Their results indicate that the wind speed affect the cooling effect: the greater the wind speed is, the better the cooling effect [21].

Furthermore, thermal stress analysis also takes an import role in the investigation of the dye-sensitized solar cell. Saasaoui et al. studied the electrical characterization of natural DSSC applying different thermal stress conditions [22]. Investigation under extended thermal stress was also conducted by Yadav et al. [23]. Bari et al. also investigated the thermal stresses of the DSSC device by using climatic chamber at a constant temperature. Their investigation showed that the degradation reduces the photogenerated current [24]. Solanki et al. investigated a concentrator PV module, in which the cell is integrated in V-troughs, resulting better heat dissipation [25]. Kim et al. improved heat dissipation in crystalline silicon PV by using a highly thermal conducting backsheet [26]. Shao et al. investigated the optical and thermal performance of dynamic concentrating solar module [27].

In previous publications, dye-sensitized solar cell – thermoelectric generator (DSSC-TEG) hybrid system, was investigated and the results showed that the use of TEG dissipated heat from the backside of the solar cell by temperature difference in the two sides. This way the thermoelectric generator can increase the efficiency of the system [28]. This article explores another method optimizing the thermal properties of the dye-sensitized solar cell. The aim of this article is to simulate the temperature distribution of the glass substrate of a dye-sensitized solar cell by modifying the glass structure with heat dissipation spheres. Applying this feature, DSSC remains transparent, and its heat dissipation can be increased. This study paves the way in providing some key insights related to this field.

2 Modelling and Simulation

During the simulation, the thermal analysis of the dye-sensitized solar cell was investigated by modifying the glass substrate. As a first step, the geometry and material were selected, then adding the physics and the mesh. As a next step, the simulations were performed, data were collected, results were analyzed, and conclusions were drawn.

COMSOL Multiphysics software was used to build the model and simulate it. COMSOL is often used for thermal analysis of various devices [29]. The simulation was in three-dimensional scheme via numerically solved coupled models. On the other hand, in the simulation steady state conditions have been applied which means that for the heat transfer the temperature does not change with time; for the fluid dynamics, the fluids flow does not change with time. In many studied literature, stationary condition is favorable for the simulations [17] [29].

2.1 Geometry and Materials

As it was mentioned, the conventional dye-sensitized solar cell contains five main components. In the preparation of the simulation design, some simplifications were made: DSSC solar cell was substituted by the glass carrier because the glass carrier constitute a significant portion of the mass of the DSSC.

During the definition of geometries, it was taken into account that the research could be continued further investigation in the future (e.g., comparison with another geometry structure). Therefore, the dimensions of the glass block (represents the dye-sensitized solar cell) are 6 mm × 4 mm × 4 mm. The dimensions are given in the following format: Width × Depth × Height. The glass block is in the middle, and it is surrounded by a block of air. At the bottom of the glass carrier, heat dissipation balls are located, with diameters of 1 mm. Thus, the system remains transparent. The glass block and the six pieces of spheres are built together. In other words, the number of the dissipation balls are six.

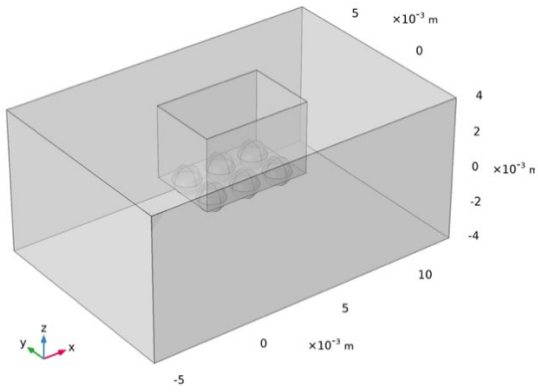

Figure 1

The designed and built geometry in three dimensions. The glass block is in the middle, and it is surrounded by the air. Also, at the bottom of the glass, heat dissipation balls are located.

The following aspects have been taken into consideration in the selection of dissipation ball diameter:

(i) The 1 mm diameter can provide sufficient surface area for efficient heat dissipation without affecting the materials' transparency

(ii) The computational time of the simulation is shorter with 1 mm diameter, with larger balls, the computational load would increase

(iii) More dissipation balls can be placed under the surface. The dimension of the air block is 18 mm × 12 mm × 8 mm. Figure 1 represents the designs and the built geometry in three dimensions, where the dimension of the three axes, are set in mm.

The air is taken into account as an incompressible fluid if the flow velocity is below 100 m/s [17] [30]. The selected materials, such as glass and air, are from COMSOL library. These built-in-materials contain the dynamic viscosity, ratio of specific heat, heat capacity at constant pressure, density and thermal conductivity.

2.2 Heat Transfer

The heat transfer module has been added to physics. From the heat transfer module, heat transfer in solids and fluid joint interfaces have been chosen.

2.2.1 Heat Transfer in Solids

The heat conduction in solid is described by the Fourier equation, where the heat transfers from the higher temperature point to the lower temperature point. The accumulated heat inside the system has to be transported in order to reduce the temperature of the cell. Thus, simulating the heat transfer in solids are essential. The following equation describes the heat transfer in solid:

$$\rho C_p \left(\frac{\partial T}{\partial t} + u_{trans} \cdot \nabla T\right) + \nabla \cdot (q + q_r) = -\alpha T : \frac{dS}{dt} + Q \quad (1)$$

Where,

- ρ is the density
- C_p is the specific heat at constant stress
- T is the absolute temperature
- u_{trans} is the velocity vector of translation motion
- q is the heat flux by conduction
- q_r is the heat flux by radiation
- α is the coefficient of thermal expansion
- S is the second Piola-Kirchhoff stress tensor
- Q contains additional heat sources

From equation (1), it is seen that the temperature and the second Piloa-Kirchhoff stress tensor are time dependent. Taking into account that the simulation is stationary, these elements in the equation is considered to zero. In other words, the first derivative of the temperature with respect to time is zero, and the first derivative of the second Piloa-Kirchhoff stress tensor with respect to time is zero. Surface-to-Ambient Radiation boundary condition has been applied between the solid surface and the fluid surface contact. The surface emissivity was 0.85 [31]. Moreover, heat flux boundary condition has been added and general inward heat flux was selected and the value of it is 1000 W/m^2.

2.2.2 Heat Transfer in Fluids

Taking into consideration the solar cell is surrounded by air, the simulation of heat transfer in fluids are also crucial. Compressible and incompressible fluids are distinguished. If the flow velocity of the fluid is below 100 m/s, the air can be considered as incompressible fluid [17], which means that the density of the fluid is constant. In other words, the density of the fluid does not change in time and with the flow. On the other hand, the following equation, equation (2), describes the incompressible fluid in three-dimensional version:

$$\frac{\partial \rho}{\partial x} = 0; \frac{\partial \rho}{\partial y} = 0; \frac{\partial \rho}{\partial z} = 0 \tag{2}$$

Where,

- ρ is the density
- x, y, z are the three-dimension coordinates

$$\rho C_p \left(\frac{\partial T}{\partial t} + u \cdot \nabla T\right) + \nabla \cdot (q + q_r) = Q_p + Q_{vd} + Q \tag{3}$$

where $Q_p = \alpha_p T \left(\frac{\partial p}{\partial t} + u \cdot \nabla p\right)$ and $Q_{vd} = t{:}\nabla u$, where,

- The dependent variables are the temperature, T
- Pressure, p

In equation (3), ρ represents the density:

- C_p is the specific heat capacity at constant pressure
- u is the velocity vector
- α_p is the coefficient of thermal expansion
- q is the heat flux by conduction
- q_r is the heat flux by radiation
- τ is the viscous stress tensor
- Q is the heat source

On the other hand, $\alpha_p = -\frac{1}{\rho}\frac{\partial \rho}{\partial T}$. Furthermore, the heat flux boundary condition has been added to the simulation. Convective heat flux has been chosen and the heat transfer coefficient was set to be 5 W/(m^2 K) and the external temperature was set to ambient temperature. The time-dependent variables appealing in the third equation are also zero, because the simulation is solved in stationary mode.

2.3 Turbulent Flow

From the single-phase flow interfaces, turbulent flow, $k-\varepsilon$ interface was selected. The program solves the Raynolds-averaged Navier-Stokes equations for the velocity field, pressure and the turbulent viscosity. According to [32], the $k-\varepsilon$ model is one of the most used turbulent models for industrial applications. The model contains two dependent variables which are the turbulent kinetic energy, namely k, and the turbulent dissipation rate, known as ε; and two additional transport equation, equation (5) and equation (7).

The turbulent viscosity is modelled as:

$$\mu_T = \rho C_\mu \frac{k^2}{\varepsilon} \tag{4}$$

where C_μ is the model constant.

On the other hand, the transport equation for k is the following:

$$\rho \frac{\partial k}{\partial t} + \rho u \cdot \nabla k = \nabla \cdot \left(\left(\mu + \frac{\mu_T}{\sigma_k} \right) \nabla k \right) + P_k - \rho \varepsilon \tag{5}$$

where the production term i:

$$P_k = \mu_T \left(\nabla u : (\nabla u + (\nabla u)^T) - \frac{2}{3}(\nabla \cdot u)^2 \right) - \frac{2}{3}\rho k \nabla \cdot u \tag{6}$$

The transport equation for ε reads:

$$\rho \frac{\partial \varepsilon}{\partial t} + \rho u \cdot \nabla \varepsilon = \nabla \cdot \left(\left(\mu + \frac{\mu_T}{\sigma_\varepsilon} \right) \nabla \varepsilon \right) + C_{\varepsilon 1} \frac{\varepsilon}{k} P_k - C_{\varepsilon 2} \rho \frac{\varepsilon^2}{k} \tag{7}$$

Constant values are determined in the moles such as $C_\mu = 0.09$, $C_{\varepsilon 1} = 1.44$, $C_{\varepsilon 2} = 1.92$, $\sigma_k = 1.0$, $\sigma_\varepsilon = 1.3$

Furthermore, two boundary conditions have been applied: (i) inlet boundary condition and (ii) outlet boundary condition. Similar to the previous points, the current equation was also solved in a stationary mode.

2.4 Mesh

After defining the parameters, building the geometries, selecting the used materials and applying the useful physics, the next step was to set the mesh. In the mesh builder, physics-controlled mesh was selected under sequence type and the element size was set to normal.

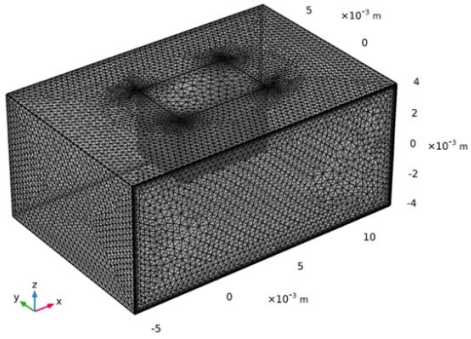

Figure 2
Mesh about the built geometry. The element size was set to normal and it is seen that the element size is much dense at the connections.

Figure 2 represents the mesh about the built geometries. The choice of the element size was made because of the computation time and computation capacity had to be taken into account. Moreover, the mesh is dense at the connection points. For the simulation Dell laptop with Intel64 Family 6 Model 141 Stepping 1, 6 cores CPU with 8 GB RAM was used. The computation time was 1 hour 59 minutes and 40 seconds.

3 Results and Discissions

The simulation aimed to explore and analyze the temperature distribution of the glass substrate of a dye-sensitized solar cell by modifying the glass substrate with heat dissipation spheres. In the following subsections, results of the temperature distribution will be shown, then the data preprocessing comes. Additionally, results from the simulation will be used for further dye-sensitized solar cell simulation. The findings provide a comprehensive understanding of the system's behavior and pave the way for potential further research in the dye-sensitized solar cell optimization filed.

Simulations were run without heat dissipation spheres at the back contact. Comparing the results, it can be stated that the dissipation balls assist in heat dissipation since the volume temperature becomes lower (from $\sim 319\ K\ to \sim 317\ K$) in stationary mode.

3.1 Results of the Simulation

The temperature distribution in the volume and in the surface, pressure distribution in the volume and velocity distribution in the volume will be presented in this subchapter. Figure 3 shows the temperature distribution across the three-dimensional geometry with the streamline.

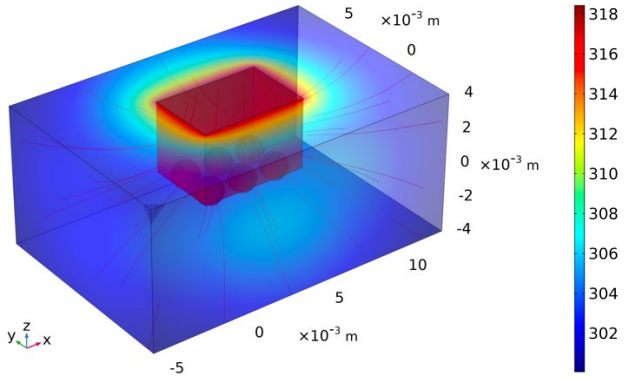

Figure 3
Temperature distribution across the three-dimensional geometry with streamline. Streamlines represent the flow of the heat.

It is visible from the figure that the central part heats the entire geometry and the heat transports from the higher temperature point to the lower temperature point. Also, in the figure, the streamlines are visible and show the direction of the heat. On the right side of the figure, the color legend, and on the left side of the figure the axis orientation can be seen. The dimension of the temperature is in kelvin. Furthermore, because of the glass substrate surrounded by the air, the air can dissipate a great part of heat from the glass substrate.

On the other hand, the glass body is higher than 316 K. Moreover, the 2D surface plot represents a cross-section view of the geometry. The mentioned surface plot is shown in Figure 4, and it shows the temperature distribution in two dimension.

It is worth mentioning that the surface plot represents the temperature distribution of the geometries better. Additionally, the added spheres contribute to the greater heat dissipation. The color mapping in both Figures 3 and 4 plots help visualize the intensity of the temperature variable indicating the warmer temperature points and the colder temperature points. For the visualization XZ-planes have been added.

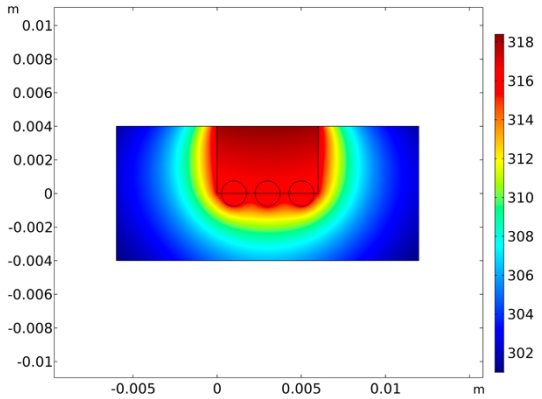

Figure 4

A cross-section wire of the geometries indicating the temperature values via the color bar on the right side of the figure. The figure represents the XZ-cut plane section of Figure 3 plot.

Moreover, in order to enhance the evaluation of the results, the pressure distribution plot can be observed in Figure 5. Additionally, it shows how the pressure changes within the system.

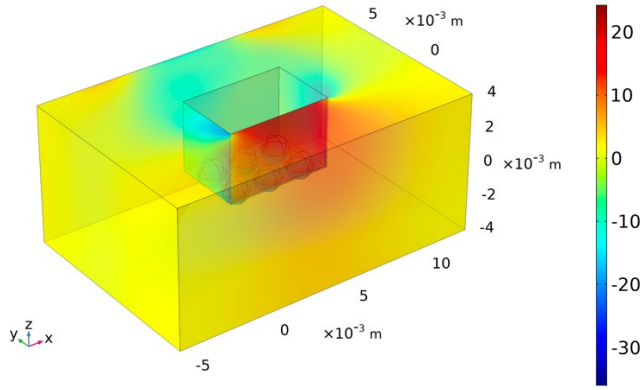

Figure 5

Pressure distribution across the three-dimensional geometry. On the right side, the color bar is visible. (Reddish color means warmer areas.)

The incoming air flows in from the front side. Therefore, the pressure values are higher in the front side, representing reddish color. Moreover, from Figure 5 it can be seen that at the edges of the air block (high block surrounds the glass block), the value of the pressure is either zero or approached to zero. The other figure which represents the turbulent flow in the materials can be observed in the Figure 5.

Figure 6 illustrates the change in velocity in the geometry. The y-component of the velocity is shows in the figure. It displays how the velocity fluctuates over the material structure. Furthermore, value of the system seems to be higher at certain regions, while in other areas, the value of the velocity is lower. In those regions where the velocity is higher, those areas indicating faster motion. The visual representation of the y-component of the velocity across the geometry provides insight into the distribution of the velocity and helps to understand how the air flows in such geometries behaves throughout the designed and built system.

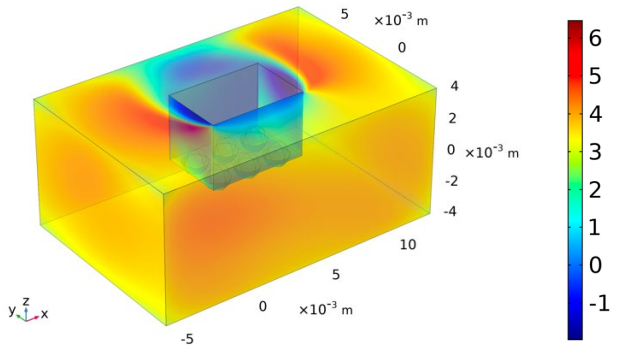

Figure 6
They y-component of the velocity across the geometry where the turbulent flow was applied. (Red color means warmer areas.)

3.2 Data Preprocessing

After the simulation and temperature distribution, pressure distribution and y-component of the velocity distribution visualizations, a cut-line 2D from the cut plane data set has been added. The starting point of the x component (point 1) of the line is 3 mm, and the finishing point of it (point 2) is 3 mm. Additionally, the starting point of the y component (point 1) is -4 mm and the finishing point of it (point 2) is 4 mm. Figure 7a, shows the aforementioned cut line used for further data visualization and Figure 7b, represents the temperature distribution across the cut line. The cut line was extracted from the three-dimensional geometry shown in Figure 7a). Moreover, Figure 7b, provides insight into how the temperature variable with distance changes. It can be seen that the part, at 0.008 mm height, has the highest temperature. The temperature gradient can be identified and also one of the key regions of interest in the plot is at 0.003, where the two geometries (glass substrate and air) meet.

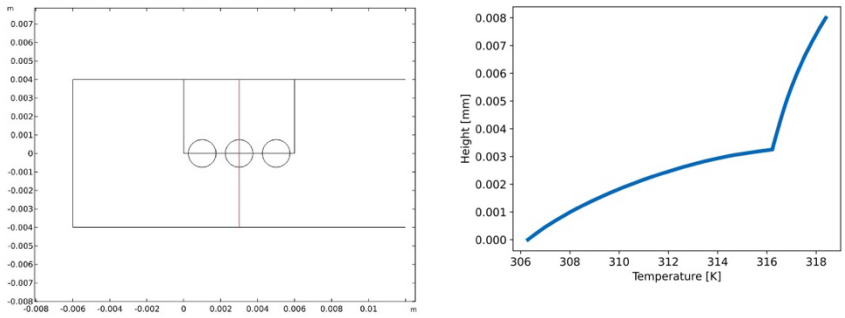

a) *b)*

Figure 7

a) The cut line used for further data visualization and data analyzation, where the horizontal coordinates are the x coordinate and the vertical coordinates are the z coordinates. b) Temperature distribution across the cut plane. The horizontal coordinates are the temperature in kelvin dimension and the horizontal coordinates are the height in millimeter dimension.

3.3 Open-Circuit Voltage

Further investigations were conducted based on the temperature results obtained from the simulation. Temperature is a crucial factor of the solar cell investigation. In the [33] publication, an application has been developed to investigate the open-circuit voltage value, which takes into consideration the experimental data and the optical equations of the dye-sensitized solar cell using numerical finite element method as numerical procedure. The input parameters are the thickness of the cell, reflection, electron density in the dark, energy between the conduction band and the Fermi level, electron lifetime and the cell temperature. Furthermore, photoncount-wavelength spectrum, transmission-wavelength spectrum and the irradiation intensity-wavelength spectrum can be imported from a .txt file. The open-circuit voltage simulation was conducted based on the result from Figure 7b. In other words, 316 K and 318 K temperature values have been taken into account for further investigation. After adding the temperature value to the application, the solved open-circuit values are 448 mV if the temperature is 318 K, and 452 mV if the temperature value is 316 K. From the results it is seen that, if the temperature increases, the open-circuit voltage would decrease. Moreover, the temperature gradient is $-2\ mV/°C$.

Conclusions

This article explores a novel method to optimize the thermal properties of dye-sensitized solar cells. In an earlier publication, the optimization of the dye-sensitized solar cell was focused on applying machine learning techniques. The aim of this article is simulating the temperature distribution of the glass substrate, of a

dye-sensitized solar cell, by modifying the glass structure with heat dissipation spheres. Applying this feature, the dye-sensitized solar cell remains transparent and its heat dissipation can be increased. Also, simulations were run without heat dissipation spheres at the black contact. Comparing the results, it can be stated that the dissipation balls assist in heat dissipation (from $\sim 319\ K$ to $\sim 317\ K$), since the volume temperature becomes lower. For the simulation, the COMSOL Multiphysics Software has been used with a three-dimensional scheme, via numerically solved coupled models – heat transfer in solids and fluids, and turbulent flow – in stationary mode have been applied.

The temperature distribution in the volume and at the surface, pressure distribution in the volume and y-component of velocity distribution in the volume, have been presented. Furthermore, the temperature distribution along a line, is extracted from the three-dimensional geometry, to analyze the thermal behaviors and used for open-circuit voltage simulation. The results show that the glass body temperature is between $316\ K - 318\ K$, resulting in $448\ mV - 452\ mV$ open-circuit voltage. On the other hand, if the temperature increases, the open-circuit voltage parameter decreases. The results obtained from the simulations, provide an opportunity for enhancing the short-circuit voltage of the dye-sensitized solar cell, through the applied application.

References

[1] S. J. Davis and K. Caldeira, 'Consumption-based accounting of CO2 emissions', *Proceedings of the National Academy of Sciences*, Vol. 107, No. 12, pp. 5687-5692, Mar. 2010, doi: 10.1073/pnas.0906974107

[2] A. M. Omer, 'Energy, environment and sustainable development', *Renewable and Sustainable Energy Reviews*, Vol. 12, No. 9, pp. 2265-2300, Dec. 2008, doi: 10.1016/j.rser.2007.05.001

[3] B. Beszédes, K. Széll, and G. Györök, 'Redundant Photo-Voltaic Power Cell in a Highly Reliable System', *Electronics*, Vol. 10, No. 11, p. 1253, May 2021, doi: 10.3390/electronics10111253

[4] O. Shvets, M. Seebauer, A. Naizabayeva, and A. Toleugazin, 'Monitoring and Control of Energy Consumption Systems, using Neural Networks', *ACTA POLYTECH HUNG*, Vol. 20, No. 2, pp. 125-144, 2023, doi: 10.12700/APH.20.2.2023.2.7

[5] M.-E. Ragoussi and T. Torres, 'New generation solar cells: concepts, trends and perspectives', *Chem. Commun.*, Vol. 51, No. 19, pp. 3957-3972, 2015, doi: 10.1039/C4CC09888A

[6] A. K. Pandey, V. V. Tyagi, J. A. Selvaraj, N. A. Rahim, and S. K. Tyagi, 'Recent advances in solar photovoltaic systems for emerging trends and advanced applications', *Renewable and Sustainable Energy Reviews*, Vol. 53, pp. 859-884, Jan. 2016, doi: 10.1016/j.rser.2015.09.043

[7] B. Beszédes, K. Széll, and G. Györök, 'A Highly Reliable, Modular, Redundant and Self-Monitoring PSU Architecture', *ACTA POLYTECH HUNG*, Vol. 17, No. 7, pp. 233-249, 2020, doi: 10.12700/APH.17.7.2020.7.13

[8] I. Diahovchenko, M. Kolcun, Z. Čonka, V. Savkiv, and R. Mykhailyshyn, 'Progress and Challenges in Smart Grids: Distributed Generation, Smart Metering, Energy Storage and Smart Loads', *Iran J Sci Technol Trans Electr Eng*, Vol. 44, No. 4, pp. 1319-1333, Dec. 2020, doi: 10.1007/s40998-020-00322-8

[9] X. Li, H. Liao, Y.-F. Du, C. Wang, J.-W. Wang, and Y. Liu, 'Carbon dioxide emissions from the electricity sector in major countries: a decomposition analysis', *Environ Sci Pollut Res*, Vol. 25, No. 7, pp. 6814-6825, Mar. 2018, doi: 10.1007/s11356-017-1013-z

[10] J. Gong, K. Sumathy, Q. Qiao, and Z. Zhou, 'Review on dye-sensitized solar cells (DSSCs): Advanced techniques and research trends', *Renewable and Sustainable Energy Reviews*, Vol. 68, pp. 234-246, Feb. 2017, doi: 10.1016/j.rser.2016.09.097

[11] R. Ghabour and P. Korzenszky, 'Dynamic Modelling and Experimental Analysis of Tankless Solar Heat Process System for Preheating Water in the Food Industry', *ACTA POLYTECH HUNG*, Vol. 20, No. 4, pp. 65-83, 2023, doi: 10.12700/APH.20.4.2023.4.4

[12] N. Ngoc Son and L. The Vinh, 'Parameter Estimation of Photovoltaic Model, Using Balancing Composite Motion Optimization', *ACTA POLYTECH HUNG*, Vol. 19, No. 11, pp. 27-46, 2022, doi: 10.12700/APH.19.11.2022.11.2

[13] K. Sharma, V. Sharma, and S. S. Sharma, 'Dye-Sensitized Solar Cells: Fundamentals and Current Status', *Nanoscale Res Lett*, Vol. 13, No. 1, p. 381, Dec. 2018, doi: 10.1186/s11671-018-2760-6

[14] Y. Li, L. Li, W. Deng, D. Zhu, and L. Hong, 'Building Integrated Photovoltaic (BIPV) Development Knowledge Map: A Review of Visual Analysis Using CiteSpace', *Buildings*, Vol. 13, No. 2, p. 389, Jan. 2023, doi: 10.3390/buildings13020389

[15] M. Onodera *et al.*, 'Modeling of Dye-Sensitized Solar Cells Based on TiO_2 Electrode Structure Model', *Jpn. J. Appl. Phys.*, Vol. 49, No. 4, p. 04DP10, Apr. 2010, doi: 10.1143/JJAP.49.04DP10

[16] S. Bose, V. Soni, and K. R. Genwa, 'Recent Advances and Future Prospects for Dye Sensitized Solar Cells: A Review', Vol. 5, No. 4, p. 9, 2015

[17] Z. Arifin, S. Suyitno, D. D. D. P. Tjahjana, W. E. Juwana, M. R. A. Putra, and A. R. Prabowo, 'The Effect of Heat Sink Properties on Solar Cell Cooling Systems', *Applied Sciences*, Vol. 10, No. 21, p. 7919, Nov. 2020, doi: 10.3390/app10217919

[18] K. G. Baiju, B. Murali, R. Subba Rao, K. Jayanarayanan, and D. Kumaresan, 'Heat sink assisted elevated temperature sintering process of TiO2 on polymer substrates for producing high performance flexible dye-sensitized solar cells', *Chemical Engineering and Processing - Process Intensification*, Vol. 149, p. 107817, Mar. 2020, doi: 10.1016/j.cep.2020.107817

[19] Y. J. Kim *et al.*, 'Dye-Sensitized Solar Cell–Thermoelectric Hybrid Generator Utilizing Bipolar Conduction in a Unified Element', *ACS Appl. Energy Mater.*, Vol. 3, No. 5, pp. 4155-4161, May 2020, doi: 10.1021/acsaem.0c00513

[20] H. Chang, M.-J. Kao, K.-C. Cho, S.-L. Chen, K.-H. Chu, and C.-C. Chen, 'Integration of CuO thin films and dye-sensitized solar cells for thermoelectric generators', Current Applied Physics, Vol. 11, No. 4, pp. S19-S22, Jul. 2011, doi: 10.1016/j.cap.2010.12.039

[21] S. Chen *et al.*, 'Numerical model analysis of thermal performance for a dye-sensitized solar cell module', *J. Phys. D: Appl. Phys.*, Vol. 46, No. 48, p. 485106, Dec. 2013, doi: 10.1088/0022-3727/46/48/485106

[22] S. Saadaoui, A. Torchani, M. A. B. Youssef, and R. Gharbi, 'Fabrication, modeling and electrical characterization of natural dye sensitized solar cell under different thermal stress conditions', *Optik*, Vol. 127, No. 20, pp. 10058-10067, Oct. 2016, doi: 10.1016/j.ijleo.2016.07.092

[23] S. K. Yadav, S. Ravishankar, S. Pescetelli, A. Agresti, F. Fabregat-Santiago, and A. Di Carlo, 'Stability of dye-sensitized solar cells under extended thermal stress', *Phys. Chem. Chem. Phys.*, Vol. 19, No. 33, pp. 22546-22554, 2017, doi: 10.1039/C7CP04598K

[24] D. Bari *et al.*, 'Thermal stress effects on Dye-Sensitized Solar Cells (DSSCs)', *Microelectronics Reliability*, Vol. 51, No. 9-11, pp. 1762-1766, Sep. 2011, doi: 10.1016/j.microrel.2011.07.061

[25] C. Solanki, C. Sangani, D. Gunashekar, and G. Antony, 'Enhanced heat dissipation of V-trough PV modules for better performance', *Solar Energy Materials and Solar Cells*, Vol. 92, No. 12, pp. 1634-1638, Dec. 2008, doi: 10.1016/j.solmat.2008.07.022

[26] N. Kim, D. Kim, H. Kang, and Y.-G. Park, 'Improved heat dissipation in a crystalline silicon PV module for better performance by using a highly thermal conducting backsheet', *Energy*, Vol. 113, pp. 515-520, Oct. 2016, doi: 10.1016/j.energy.2016.07.046

[27] Z. Shao, B. Wang, L. Cai, C. Chang, and L. Sun, 'Optical and thermal performance of dynamic concentrating solar module for building integration', *Journal of Cleaner Production*, Vol. 367, p. 132931, Sep. 2022, doi: 10.1016/j.jclepro.2022.132931

[28] Z. Varga and E. Racz, 'Machine Learning Analysis on the Performance of Dye-Sensitized Solar Cell—Thermoelectric Generator Hybrid System', *Energies*, Vol. 15, No. 19, p. 7222, Oct. 2022, doi: 10.3390/en15197222

[29] P. Saxena and N. E. Gorji, 'COMSOL Simulation of Heat Distribution in Perovskite Solar Cells: Coupled Optical–Electrical–Thermal 3-D Analysis', *IEEE J. Photovoltaics*, Vol. 9, No. 6, pp. 1693-1698, Nov. 2019, doi: 10.1109/JPHOTOV.2019.2940886

[30] J.-H. Kim, S.-H. Park, and J.-T. Kim, 'Experimental Performance of a Photovoltaic-thermal Air Collector', *Energy Procedia*, Vol. 48, pp. 888-894, 2014, doi: 10.1016/j.egypro.2014.02.102

[31] R. Gardon, 'The Emissivity of Transparent Materials', *J American Ceramic Society*, Vol. 39, No. 8, pp. 278-285, Aug. 1956, doi: 10.1111/j.1151-2916.1956.tb15833.x

[32] V. Guimet and D. Laurence, 'A LINEARISED TURBULENT PRODUCTION IN THE k-ε MODEL FOR ENGINEERING APPLICATIONS', in *Engineering Turbulence Modelling and Experiments 5*, Elsevier, 2002, pp. 157-166, doi: 10.1016/B978-008044114-6/50014-4

[33] Z. Varga and E. Racz, 'Application Development with Finite Element Method to Calculate Photogeneration Rate and Open-Circuit Voltage of Dye Sensitized Solar Cell', *Syst. Theor. Control Comput. J.*, Vol. 2, No. 2, pp. 17-24, Dec. 2022, doi: 10.52846/stccj.2022.2.2.39